

A Low-Power and High-Precision Programmable Analog Filter Bank

Brandon Rumberg, *Student Member, IEEE*, and David W. Graham, *Member, IEEE*

Abstract—Analog filter banks benefit remote audio- and vibration-sensing applications, which require frequency analysis to be performed with low-power consumption and with moderate-to-high precision. The precision of a filter bank depends on both the signal-path precision (i.e., dynamic range) and also the parameter precision (e.g., accuracy of the center frequencies). This brief presents a new bandpass filter for audio-frequency filter banks and provides a procedure for designing this filter. The filter is used in a 16-channel filter bank which has been fabricated in a 0.35- μm CMOS process. This filter bank has a dynamic range exceeding 62 dB and consumes only 63.6 μW when biased for speech frequencies. The filter bank's parameters are set via floating-gate current sources. This brief shows how to use these floating gates to obtain a versatile filter bank that can be precisely reprogrammed to arbitrary filter spacings and frequency weightings, with a parameter accuracy exceeding 99%.

Index Terms—Bandpass filters, CMOS analog integrated circuits, spectral analysis, programmable filters.

I. INTRODUCTION

DUE to the dynamic vibrational nature of many phenomena, sensor-processing applications often decompose signals into a time–frequency representation for analysis, manipulation, or recognition of the signal. Time-frequency representations characterize changes in the signal's spectrum over time and are typically implemented in two main ways: 1) a constant-bandwidth representation such as the short-time Fourier transform, which provides the most compact representation for signals with long-term periodicity and 2) a constant-relative-bandwidth or scale-space representation such as the wavelet transform, which provides the most compact representation for signals with localized time-frequency components [1]. Time-frequency analysis can be performed efficiently with analog filter banks [2], which naturally yield a scale-space representation [3]. Integrated analog filter banks were incubated in the research of silicon cochleae [4]–[8], and their low-power operation makes them well suited to battery-powered applications such as cochlear implants [9], [10] and wireless sensor networks [11].

In order for analog filter banks to be an option for incorporation into mature systems, they should operate with high precision, and their filter parameters should be reprogrammable. The precision of a filter bank is affected by both the signal-path precision (e.g., dynamic range) and the parameter

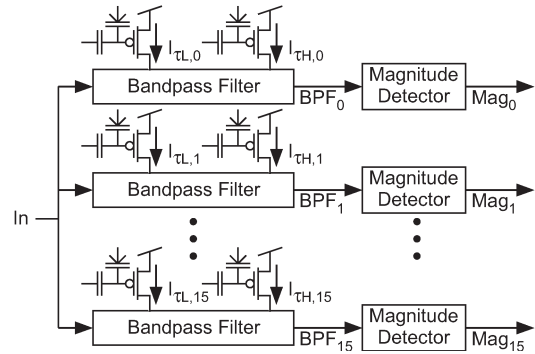


Fig. 1. Block diagram of our analog filter bank chip, which combines a parallel array of bandpass filters with subband magnitude detectors. Each circuit parameter is controlled independently via floating-gate current sources, thus achieving precise control of the filter bank's settings.

precision (e.g., center frequencies and bandwidths). A large dynamic range is difficult to achieve in low-power circuits due to the relatively high noise levels and reduced voltage headroom [7]. Precise tuning of filter parameters is difficult to achieve in compact and low-power circuits due to process variations, which can be partially overcome by using large device sizes and additional circuitry. Nevertheless, state-of-the-art filter banks have center-frequency errors $>10\%$ [5]. Previous filter banks have been demonstrated to achieve either a large dynamic range [10] or precise and reprogrammable parameters [12], but in this brief, we present a filter bank which achieves both a large dynamic range and is also precise and programmable, while maintaining low-power consumption.

Fig. 1 shows the block diagram of our 16-channel filter bank chip, which was fabricated in a standard 0.35- μm CMOS process. The filter bank performs time–frequency analysis with a parallel array of bandpass filters. For the bandpass filter, we use our new operational transconductance amplifier (OTA)-based capacitively coupled current conveyor (C^4), which significantly improves upon the shortcomings of the transistor-based version [13]. In Section 2, we present this bandpass filter, demonstrate its large dynamic range, and provide a design procedure. To achieve precise programmability at low-power operation, we set the filter bank parameters with floating-gate-based current sources (i.e., nonvolatile analog memory), which have been shown to be a good option for achieving precise and programmable biasing in CMOS circuits [12]. Through the use of floating-gate transistors, we have consistently achieved a percent error below 1% when programming the center frequencies, gains, and bandwidths of the filters. In Section 3, we demonstrate the precise programmability of the filter bank by programming it to different filter spacings and frequency weightings. All plots in this brief are measurements from the fabricated filter bank.

Manuscript received September 23, 2011; revised December 9, 2011; accepted February 12, 2012. Date of publication March 12, 2012; date of current version April 11, 2012. This work was supported in part by GTronix, Inc. This paper was recommended by Associate Editor R. Martins.

The authors are with the Lane Department of Computer Science and Electrical Engineering, West Virginia University, Morgantown, WV 26506 USA (e-mail: brumberg@mix.wvu.edu; david.graham@mail.wvu.edu).

Digital Object Identifier 10.1109/TCSII.2012.2188460

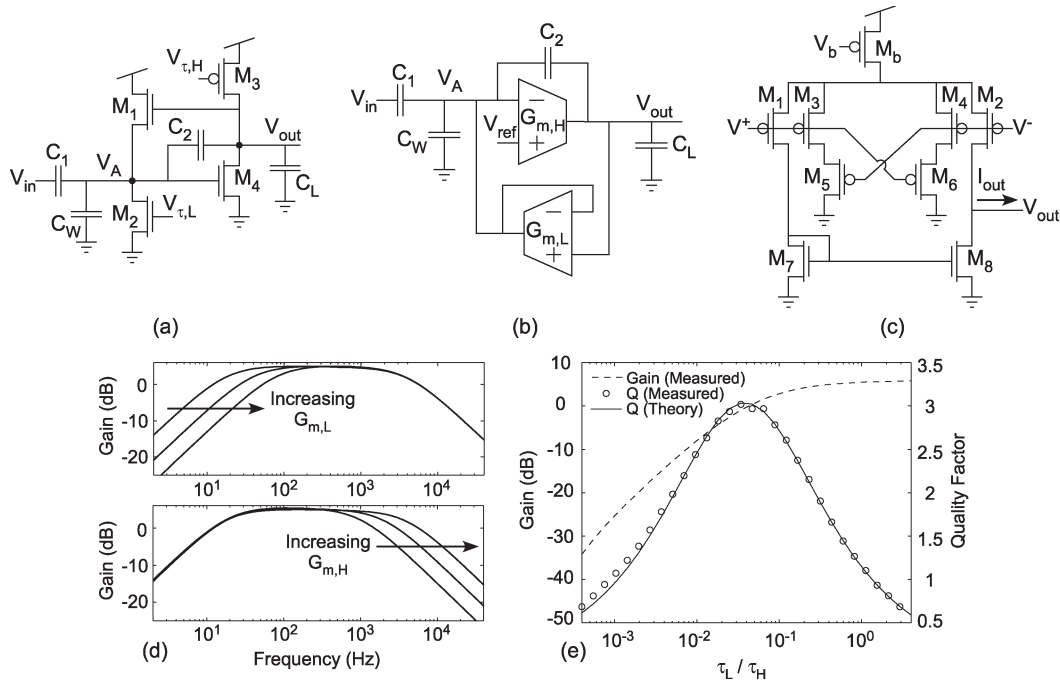


Fig. 2. (a) Original-transistor-based C^4 . (b) New OTA-based C^4 . (c) Symmetric “bump”-linearized transconductor that is used in the OTA- C^4 . (d) Measured frequency responses of the OTA- C^4 . The independence of the corner frequencies is demonstrated by stepping one bias at a time. (e) Measured gain and Q of the OTA- C^4 , both plotted as a function of the time constant ratio τ_l/τ_h , which is proportional to $G_{m,H}/G_{m,L}$.

II. BANDPASS FILTER

Transconductance–capacitance (G_m – C) topologies are a common choice for low-power integrated filters. When low-power operation is required, G_m – C filters can be operated in the subthreshold domain. Since OTAs have low transconductance in the subthreshold region, these filters are able to achieve the long time constants that are needed for audio-frequency operation while using small integrated capacitors, thus enabling compact designs. G_m – C filters are also good for applications requiring programmability since the transconductance values, which are easily controlled by adjusting OTA bias currents, appear in the transfer function as parameters of the filter (thus, the filter parameters are easily modified). Furthermore, since these filter parameters typically scale with center frequency, filter bank spacing is easily achieved with current ratioing or resistive dividers. For these reasons, most low-power filter banks have been based on G_m – C filters.

Unfortunately, the dynamic range of G_m – C filters is limited by the small linear range of the subthreshold differential pair. This problem is often mitigated through transconductor linearization [14], [15] or through capacitive division to keep the signal within the linear range of the transconductors [16]; we use both of these techniques in this brief. Another limitation to the dynamic range of low-power G_m – C filters is the small subthreshold current, which results in relatively high noise levels for the bandwidth and can be alleviated by increasing both the capacitor sizes and the power level.

A. OTA- C^4

The bandpass filter that we created for our filter bank is our new OTA-based capacitively coupled current conveyor (C^4) shown in Fig. 2(b). This filter is based on our previously reported transistor-based C^4 (transistor- C^4) [13], which is shown

in Fig. 2(a). The C^4 filter topology offers flexible tuning, with run-time adjustable center frequency, gain, and quality factor (Q). In the OTA-based version of the C^4 , the high-gain inverting transconductor $G_{m,H}$ replaces the common-source amplifier M_3 – M_4 , and the follower-configured transconductor $G_{m,L}$ replaces the source follower M_1 – M_2 . We have developed the OTA- C^4 to more easily increase the filter’s linear range and also to obtain control over the filter’s dc operating point.

In the OTA- C^4 , capacitors C_1 and C_W form a capacitive divider that attenuates the ac input onto the central node V_A and makes the filter’s response independent of the dc level of V_{in} . The negative feedback around $G_{m,H}$ holds V_A at a dc level of V_{ref} . In the transistor- C^4 , the source follower causes an offset in the feedback path which can shift the equilibrium point away from the center of the inverting amplifier’s linear range, reducing the filter’s linear range below the linear range of its transconductance elements. The OTA- C^4 fixes this by feeding back through a low-offset follower OTA ($G_{m,L}$).

Another problem with the transistor- C^4 is that the common-source amplifier’s quiescent point is bias dependent; this means that the output dc level of each filter in the array will be different, thereby requiring some way of correcting for these differences in order to compare/combine the outputs of different channels. The OTA- C^4 fixes this problem by using the noninverting terminal of $G_{m,H}$ to globally set the dc level of the filter bank.

Additionally, the use of OTAs makes the filter modular, offering the designer the flexibility to optimize the filter for their application, e.g., further extending the linear range or reducing the transconductance for ultralow-frequency applications. We have extended the linear range of the OTA- C^4 by using the symmetric “bump” OTA shown in Fig. 2(c) [15], which has four times the linear range of the standard differential pair.

The transfer function for the OTA-C⁴ is

$$\frac{V_{\text{out}}}{V_{\text{in}}} = -\frac{C_1}{C_2} \frac{s\tau_l(1-s\tau_f)}{1+s\left(\tau_l+\tau_f\left(\frac{C_O}{C_2}-1\right)\right)+s^2\tau_h\tau_l} \quad (1)$$

where $C_T = C_1 + C_2 + C_W$ and $C_O = C_2 + C_L$ and

$$\tau_l = \frac{C_2}{G_{m,L}} \quad \tau_h = \frac{C_O C_T - C_2^2}{C_2 G_{m,H}} \quad \tau_f = \frac{C_2}{G_{m,H}} \quad (2)$$

where τ_l is the time constant of the low corner frequency and τ_h is the time constant of the high corner frequency. These time constants are controlled independently by the transconductances $G_{m,L}$ and $G_{m,H}$, respectively, as shown in Fig. 2(d). Proper capacitor sizing ensures that the feed-through time constant τ_f is at a sufficiently high frequency such that its effect on the numerator of the transfer function can be ignored, so that the transfer function takes the familiar form of a bandpass filter.

The OTA-C⁴ is a flexible bandpass filter, with run-time tunable center frequency, gain, and Q , which are all established via the transconductances. The gain and Q both depend on the ratio $G_{m,H}/G_{m,L}$ and are specified as

$$|A_v| = \frac{C_1}{C_2} \frac{1}{1 + \frac{C_L}{C_2} \frac{G_{m,L}}{G_{m,H}}} \quad Q = \frac{\sqrt{C_T C_O - C_2^2}}{C_L \sqrt{\frac{G_{m,L}}{G_{m,H}} + C_2} \sqrt{\frac{G_{m,H}}{G_{m,L}}}} \quad (3)$$

Fig. 2(e) shows the measured gain and Q of the OTA-C⁴ for different transconductance ratios as a function of τ_l/τ_h , which is proportional to $G_{m,H}/G_{m,L}$. Equation (3) shows that the gain is highest when $G_{m,H} \gg G_{m,L}$ where it approaches a value of C_1/C_2 , which is two (6 dB) for this particular implementation. As $G_{m,H}/G_{m,L}$ decreases, the corner frequencies cross and cause the gain to decrease. The Q has a maximum value when $G_{m,H}/G_{m,L} = C_L/C_2$ and decreases symmetrically as the transconductance ratio changes. When biased for maximum Q , the gain is $|A_v| = C_1/(2C_2)$.

B. Design

We have developed an algorithmic design procedure for the OTA-C⁴ that is similar to the procedure for the transistor-C⁴ in previous work [13] but that has been modified for this new circuit. This design procedure helps the designer to choose the device sizes that are needed to achieve the desired dynamic range (DR) in decibels, maximum gain ($A_{v,\text{max}}$), and maximum Q (Q_{max}), as well as to choose the currents that are needed to achieve the desired filter characteristics. We make the following assumptions for this procedure: 1) The dynamic range requirement is met at the Q_{max} condition; 2) the maximum output amplitude ($V_{\text{out,max}}$) is equal to the linear range of the transconductors (V_L); and 3) the transconductor noise is mostly white, as is typical for subthreshold OTAs [14].

1) Choose C_2 to meet the DR specification

$$C_2 = \frac{Nq}{4V_L} 10^{\frac{DR}{10}} \quad (4)$$

where N is the number of noise sources in the transconductors [14] and q is the charge of an electron.

2) Choose C_1 either for the following: a) the desired maximum gain or b) the desired gain at the Q_{max} condition

$$C_1 = \begin{cases} C_2 A_{v,\text{max}} & (a) \\ 2C_2 A_{v,Q} & (b) \end{cases} \quad (5)$$

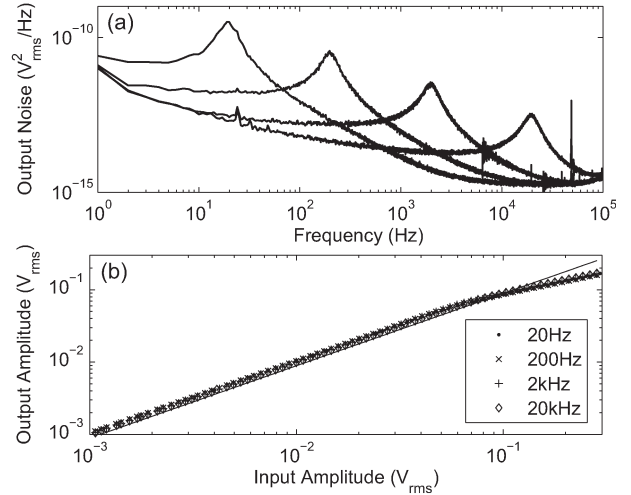


Fig. 3. (a) Measured output-referred noise of the OTA-C⁴. (b) Compression point measurement for the OTA-C⁴. The line shows the 1-dB deviation.

TABLE I
PERFORMANCE RESULTS

Metric	20Hz	200Hz	2kHz	20kHz
Noise (μV_{rms})	59.8	59.7	58.2	58.7
1dB Comp. Point (mV_{rms})	76.5	80.3	87.4	86.8
1dB Comp. Point (dBm)	-9.32	-9.00	-8.16	-8.22
1dB DR (dB)	62.1	62.6	63.5	63.4
THD at 70.7mV _{rms}	0.89%	0.89%	0.84%	0.61%
OIP3	141.4mV _{rms} ; -4.00dBm			
Power	19.0nW	198nW	2.85 μ W	75.4 μ W

- 3) Choose C_T for linearity: $C_T = 4C_2 Q_{\text{max}}^2$.
- 4) C_L should be on the same order as C_T for step 1) to be valid but can otherwise be used to position the feed-through time constant (τ_f) or to optimize for power

$$P = \frac{C_L}{V_L} V_{dd} Q_{\text{max}} f_c \quad (6)$$

- 5) Use (3) to choose the transconductance ratio ($R = G_{m,H}/G_{m,L}$) for either the desired gain or Q .
- 6) Choose the transconductance values for the desired center frequency (f_c) using

$$G_{m,L} = \sqrt{\frac{C_O C_T - C_2^2}{R}} 2\pi f_c \quad G_{m,H} = R G_{m,L} \quad (7)$$

C. Performance

Using the aforementioned design procedure, the filters for our filter bank chip were designed for a dynamic range of 60 dB, a maximum gain of 6 dB, and a maximum Q of three. The frequency response measurements in Fig. 2(d)–(e) verify that the filter meets the maximum gain and maximum Q specifications.

To verify that the fabricated filter meets the dynamic range specifications, we determined the maximum and minimum signal levels while the filter was simultaneously biased for unity gain and maximum Q . The experiments were performed at four frequencies across the audio-frequency range (20 Hz, 200 Hz, 2 kHz, and 20 kHz). The minimum signal level is

TABLE II
COMPARISON AMONG LOW-POWER SECOND-ORDER AUDIO-RANGE BANDPASS FILTERS

	Proposed	[16]	[17]	[18]	[19]	[20]
Technology	0.35 μm	1.5 μm BiCMOS	0.5 μm	0.35 μm	0.35 μm	0.8 μm
Freq. Range	20Hz–20kHz	100Hz–10kHz	700Hz–4kHz	30Hz–30kHz	100Hz–30kHz	100Hz–2kHz
DR	62.1–63.5dB	62dB	55dB	51dB	62.3dB	62–78dB
Power	19nW–75.4 μW	42nW–2 μW	1.12 μW (1kHz)	290nW (660Hz)	<16 μW	2.5 μW (2kHz)

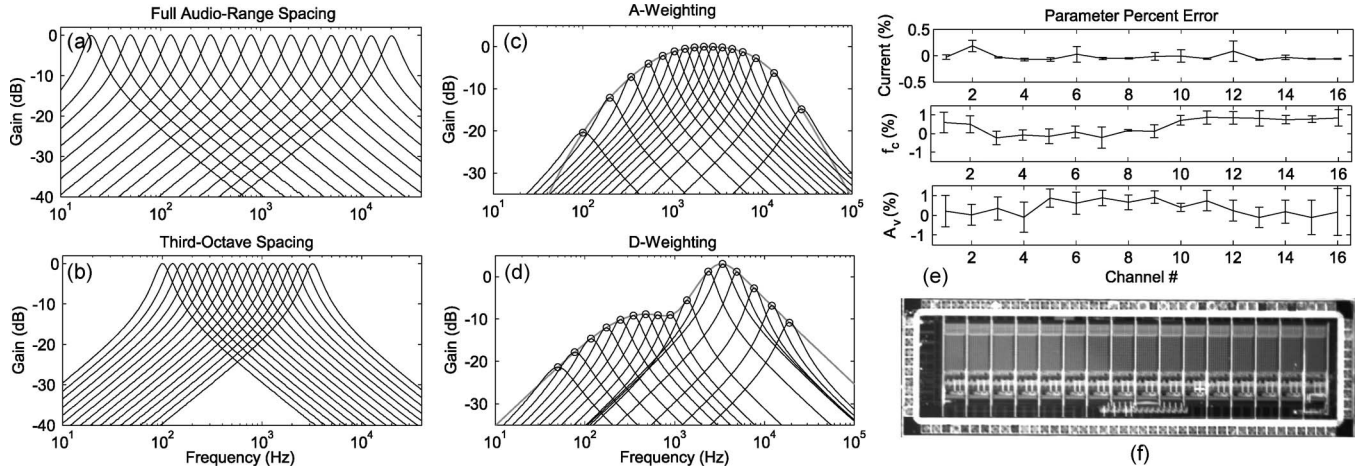


Fig. 4. Measured filter bank ac responses. (a) Biased for 20 Hz–20 kHz with unity gain. (b) Biased for unity gain and third-octave spacing starting at 100 Hz. (c) A-weighting. (d) D-weighting. The circles show the targeted gains and center frequencies. (e) Percentage error results of the four filter bank biasings in parts (a)–(d). The mean and standard deviation of the percentage error are shown for the currents, center frequency, and gain of each channel. (f) Die photograph of our filter bank chip. The chip is 4.8 mm \times 1.4 mm. The dimension of a single OTA-C⁴ is 560 μm \times 237 μm .

defined as the integrated output noise, and the maximum signal level is defined as the output-referred 1-dB compression point. The compression point is an appropriate criterion for spectral analysis applications, for which only the magnitude of the filter output is required.

The circuit was designed for a dynamic range that extends from 70.7 μV_{rms} to 70.7 mV_{rms}. The measured output-referred noise is shown in Fig. 3(a). The integrated output noise values are all well below the designed noise floor and are listed in Table I along with all other measured performance results. Fig. 3(b) shows the compression point measurements, which exceed 70.7 mV_{rms} for all cases (a 2.5-times improvement over the original C⁴[13]), yielding a dynamic range of over 62 dB for all four frequencies. To further characterize the linearity, we also measured the total harmonic distortion (THD) and the intermodulation distortion. The THD was measured to be less than 1% for 70.7-mV_{rms} inputs, and the OIP3 point was measured to be 141.4 mV_{rms} or -4 dBm (50- Ω reference).

In Table II, we compare the OTA-C⁴ with other recently reported low-power second-order voltage-mode audio-range bandpass filters. We note that three of the filters are fully differential [18]–[20] and all but one of the topologies [16] in Table II are capable of complex poles (i.e., $Q > 0.5$). In comparison to the other filters, the OTA-C⁴ achieves comparable performance and is compact with the fewest transconductors.

III. FILTER BANK

Our filter bank chip has been fabricated in a 0.35- μm CMOS process and is shown in Fig. 4(f). The filter bank has 16 parallel channels, with each channel consisting of an OTA-C⁴ and a magnitude detector, as shown in Fig. 1. Details of the

magnitude circuit are provided in [11]. In order to achieve precise programmability, we use floating-gate transistors to bias the circuits [12]; this configuration is shown in Fig. 1. Floating-gate transistors are MOSFETs that have only capacitive inputs to their gates, a structure which can be formed in standard CMOS processes. The amount of charge on the floating gate can be programmed via Fowler–Nordheim tunneling and hot-electron injection. This programmed charge is nonvolatile and provides fine control over the drain current. In order to control $G_{m,H}$ and $G_{m,L}$ using the floating-gate transistors, the floating-gate currents are copied into the transistor M_b of the OTA-C⁴ transconductors using both an nFET and a pFET current mirror.

Through the use of programmable biasing, we are able to correct for fabrication mismatch and process variations, enabling us to set the circuit parameters with very high accuracy. To correct for these variations after fabrication, we performed the following characterization routine, which has three steps. First, I_H (bias current of $G_{m,H}$) is stepped, and its associated time constant (τ_h) is measured at each step to determine the mapping between I_H and τ_h independent of component tolerances. During this step, I_L (bias current of $G_{m,L}$) is held at a low value so that the low corner frequency does not interfere with measuring the high corner frequency [see Fig. 2(d)]. Second, I_H is held at a high value (so that the high corner frequency has no effect on measurements), and I_L is stepped to determine its mapping to τ_l . Third, the ratio of τ_l/τ_h is swept, this time measuring the Q and gain, which are fit to the expressions in (3). This routine can be optimized for speed by measuring a small number of well-chosen data points. Characterization only needs to be performed once for each filter to successfully cancel out fabrication mismatch.

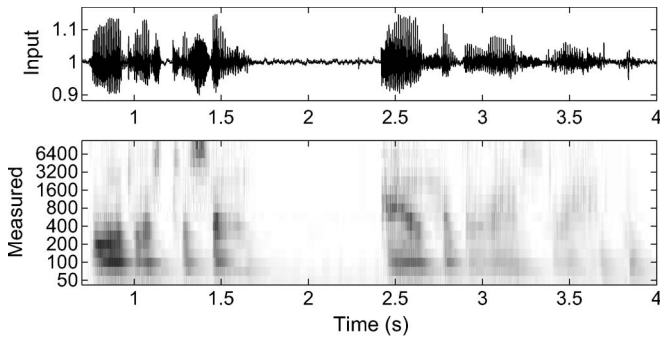


Fig. 5. Time–frequency analysis performed with the filter bank. The top subplot is the speech waveform which was streamed into the filter bank. The bottom subplot is the resulting spectral decomposition.

Once a filter has been characterized, the last two steps of the design procedure are used to determine the currents required for the desired combination of f_c and A_v or f_c and Q . The floating gates are then programmed to these currents [21] to achieve the desired filter characteristics. Our programming algorithm, which has not been optimized for speed, takes approximately 30 s/gate, and program times on the order of milliseconds have previously been reported with similar algorithms [21]. Because of the independent control of these filter parameters, the filter bank is very versatile. Independent control of each filter’s center frequency and Q enables the user to program the filter bank to cover the frequency range of interest or even to focus on specific frequencies if signal characteristics are known *a priori*. Independent control of the gain of each channel allows the user to selectively emphasize bands or to adopt common perceptually derived frequency weightings, such as A- or D-weighting, without requiring a multiplier in each band.

To verify the accuracy of the parameter programming and also to demonstrate the versatility of the filter bank, we programmed the filter bank to the following filter spacings and frequency weightings: 20 Hz–20 kHz with unity gain, third-octave spacing with unity gain, A-weighting, and D-weighting. The resulting measured ac responses are shown in Fig. 4(a)–(d). The measured accuracies of the programmed currents and parameters in Fig. 4(a)–(d) are shown in Fig. 4(e). The mean absolute percentage error across all channels is 0.087% for the currents, 0.536% for center frequency, and 0.634% for gain.

To demonstrate the filter bank performing time–frequency decomposition, we streamed a speech waveform through the filter bank, which was biased for half-octave spacing. A simulated version of the magnitude circuit was used to extract the magnitude of the measured output waveforms of the filter bank. The resulting spectral magnitude is shown in Fig. 5.

IV. CONCLUSION

We have presented a low-power and programmable analog filter bank that achieves both high signal-path precision (> 62 dB) and high parameter accuracy ($> 99\%$). Thus, this filter bank meets the requirements for inclusion in today’s demanding battery-powered audio-processing systems. Furthermore, we have illustrated the utility of using floating-gate transistors for precise, programmable, and low-power systems by demonstrating the high accuracy which can be achieved when programming arbitrary array settings.

ACKNOWLEDGMENT

The authors would like to thank P. Hasler for fabrication of the integrated circuit and B. Degnan for technical and mask-level help. The authors would also like to thank P. Smith for useful discussions related to continuous-time filters.

REFERENCES

- [1] G. Strang and T. Nguyen, *Wavelets and Filter Banks*. Wellesley, MA: Wellesley-Cambridge Press, 1996.
- [2] M. Kucic, A. Low, P. Hasler, and J. Neff, “A programmable continuous-time floating-gate Fourier processor,” *IEEE Trans. Circuits Syst. II, Analog Digit. Signal Process.*, vol. 48, no. 1, pp. 90–99, Jan. 2001.
- [3] W. Liu, M. Goldstein, Jr., and A. Andreou, “Multiresolution speech analysis with an analog cochlear model,” in *Proc. IEEE-SP Symp. Time-Freq. Time-Scale Anal.*, Victoria, BC, Canada, Oct. 1992, pp. 433–436.
- [4] B. Wen and K. Boahen, “A 360-channel speech preprocessor that emulates the cochlear amplifier,” in *Proc. IEEE ISSCC Dig. Tech. Papers*, Feb. 2006, pp. 2268–2277.
- [5] E. Fragnière, “A 100-channel analog CMOS auditory filter bank for speech recognition,” in *Proc. IEEE ISSCC Dig. Tech. Papers*, Feb. 2005, vol. 1, pp. 140–589.
- [6] S.-C. Liu, A. van Schaik, B. Minch, and T. Delbrück, “Event-based 64-channel binaural silicon cochlea with Q enhancement mechanisms,” in *Proc. IEEE Int. Symp. Circuits Syst.*, May 2010, pp. 2027–2030.
- [7] R. Sarpeshkar, R. Lyon, and C. Mead, “A low-power wide-dynamic-range analog VLSI cochlea,” *Analog Integr. Circuits Signal Process.*, vol. 16, no. 3, pp. 245–274, Aug. 1998.
- [8] A. Katsiamis, E. Drakakis, and R. Lyon, “A biomimetic, 4.5 μW , 120+dB, log-domain cochlea channel with AGC,” *IEEE J. Solid-State Circuits*, vol. 44, no. 3, pp. 1006–1022, Mar. 2009.
- [9] J. Georgiou and C. Toumazou, “A 126- μW cochlear chip for a totally implantable system,” *IEEE J. Solid-State Circuits*, vol. 40, no. 2, pp. 430–443, Feb. 2005.
- [10] M. Baker, T. Lu, C. Salthouse, J. Sit, S. Zhak, and R. Sarpeshkar, “A 16-channel analog VLSI processor for bionic ears and speech-recognition front ends,” in *Proc. IEEE CICC*, 2003, pp. 521–526.
- [11] B. Rumberg, D. Graham, V. Kulathumani, and R. Fernandez, “Hibernets: Energy-efficient sensor networks using analog signal processing,” *IEEE J. Emerg. Sel. Topics Circuits Syst.*, vol. 1, no. 3, pp. 321–334, Sep. 2011.
- [12] D. Graham, P. Smith, R. Chawla, and P. Hasler, “A programmable bandpass array using floating-gate elements,” in *Proc. IEEE Int. Symp. Circuits Syst.*, Vancouver, BC, Canada, May 2004, vol. 1, pp. I-97–I-100.
- [13] D. Graham, P. Hasler, R. Chawla, and P. Smith, “A low-power, programmable bandpass filter section for higher-order filter applications,” *IEEE Trans. Circuits Syst. I, Reg. Papers*, vol. 54, no. 6, pp. 1165–1176, Jun. 2007.
- [14] R. Sarpeshkar, R. Lyon, and C. Mead, “A low-power wide-linear-range transconductance amplifier,” *Analog Integr. Circuits Signal Process.*, vol. 13, no. 1/2, pp. 123–151, May/June 1997.
- [15] P. Furth and H. Ommani, “Low-voltage highly-linear transconductor design in subthreshold CMOS,” in *Proc. IEEE Midwest Symp. Circuits Syst.*, Sacramento, CA, Aug. 1997, vol. 1, pp. 156–159.
- [16] C. Salthouse and R. Sarpeshkar, “A practical micropower programmable bandpass filter for use in bionic ears,” *IEEE J. Solid-State Circuits*, vol. 38, no. 1, pp. 63–70, Jan. 2003.
- [17] K. Odame, D. Anderson, and P. Hasler, “A bandpass filter with inherent gain adaptation for hearing applications,” *IEEE Trans. Circuits Syst. I, Reg. Papers*, vol. 55, no. 3, pp. 786–795, Apr. 2008.
- [18] O. Omeni, E. Rodríguez-Villegas, and C. Toumazou, “A micropower CMOS continuous-time filter with on-chip automatic tuning,” *IEEE Trans. Circuits Syst. I, Reg. Papers*, vol. 52, no. 4, pp. 695–705, Apr. 2005.
- [19] L. Pylarinos and K. Phang, “Low-voltage programmable g_m - C filter for hearing aids using dynamic gate biasing,” in *Proc. IEEE Int. Symp. Circuits Syst.*, May 2005, vol. 3, pp. 1984–1987.
- [20] E. Rodríguez-Villegas, A. Yüfera, and A. Rueda, “A 1.25-V micropower G_m - C filter based on FGMOs transistors operating in weak inversion,” *IEEE J. Solid-State Circuits*, vol. 39, no. 1, pp. 100–111, Jan. 2004.
- [21] A. Bandyopadhyay, G. Serrano, and P. Hasler, “Adaptive algorithm using hot-electron injection for programming analog computational memory elements within 0.2% of accuracy over 3.5 decades,” *IEEE J. Solid-State Circuits*, vol. 41, no. 9, pp. 2107–2114, Sep. 2006.